PERGAMON

International Journal of Solids and Structures 38 (2001) 1539–1550

INTERNATIONAL JOURNAL OF SOLIDS and STRUCTURES

www.elsevier.com/locate/ijsolstr

Singular plastic fields in non-associative pressure sensitive solids

Panos Papanastasiou [a,*], David Durban [b]

[a] *Schlumberger Cambridge Research, Cambridge CB3 0EL, UK*
[b] *Faculty of Aerospace Engineering, Technion, Haifa 32000, Israel*

Received 21 July 1999; in revised form 3 March 2000

Abstract

Singular plastic fields at crack tips are investigated for a non-associative deformation theory modelling a Drucker–Prager material. Plane-strain mode-I eigensolutions are mapped over a range of material parameters along with a pure power law response. The material does not admit a strain energy function and the level of stress singularity is higher than the HRR values. The latter are recovered for associated models but, in general, the singularity reported here deviate from J-integral analysis with increasing non-associativity. Near tip profiles are illustrated for a few representative cases, indicating an increasing sensitivity to non-associativity at higher levels of the hardening exponent. © 2001 Elsevier Science Ltd. All rights reserved.

Keywords: Singular plastic fields; Singularity; Drucker–Prager; Pressure-sensitive; Non-associative material; Plane-strain; Mode-I crack

1. Background

Singular plastic stress fields engulfing crack tips have been mapped in numerous studies covering a broad spectrum of constitutive response. More specifically, crack tip fields in pressure sensitive solids have been examined in recent years for associated Drucker–Prager materials modelled by the small strain deformation theory and pure power law plastic response (Li and Pan, 1990; Yuan and Lin, 1993). Bigoni and Radi (1993) studied quasi-static crack propagation for a linear hardening elastoplastic response. As expected, for power law materials, the dominant stress singularity is that of HRR fields – a result supported by the usual argument of the path independent J-integral (Hutchinson, 1968a,b; Rice and Rosengren, 1968). The behaviour of cracks in porous solids is of interest in geomechanics within the context of hydraulic fracturing (Papanastasiou, 1997, 1999), in the analysis of sintered powder metal components, polymeric materials and ceramics.

This work aims at investigating small strain singular crack tip fields for pressure sensitive materials that are not endowed with a strain energy function. Thus, we examine mode-I plane-strain field for

* Corresponding author. Tel.: +44-1223-325202; fax: +44-1223-327019.
E-mail address: panos@cambridge.scr.slb.com (P. Papanastasiou).

0020-7683/01/$ - see front matter
PII: S0020-7683(00)00098-6

non-associative deformation theory modelling Drucker–Prager solids with pure power hardening characteristics. It is worth mentioning that geomaterials, in general, exhibit a non-associated plastic response.

The governing equations, introduced in Section 2, admit a separation of variables solution which generates an eigenvalue system of the fourth order. A numerical solution using a Galerkin finite element scheme is employed in Section 3 to trace the strongest permissible stress singularity. The eventual outcome, calculated over a range of material parameters, can be approximately described by the following expression for the radial singularity level of the stress components:

$$\frac{1}{1+n}\left[1+0.4094(\mu-\eta)-0.3455(\mu-\eta)^2+\cdots\right], \tag{1}$$

where n is the hardening exponent and $(\mu-\eta)$ is a measure of deviation from associativity. Here, μ and η are the friction and dilation coefficients, respectively. For associated solids, $\mu=\eta$, we recover the HRR singularity $1/(n+1)$, but otherwise the singularity slightly increases with non-associativity.

Sample illustrations of near tip field profiles indicate that strains and displacements are more sensitive to deviations from associativity, particularly at higher values of n.

2. Near-tip plastic field equations

With the notation displayed in Fig. 1, we examine the singular plastic field near the tip of a crack embedded in a pressure sensitive plastic solid. Far field loading is symmetrical with respect to the crack axis ($\theta=0$) and material response is constrained by plane strain conditions. We ignore the elastic constitutive branch in the vicinity of the tip assuming the small strain deformation theory model,

$$\boldsymbol{\epsilon}=\frac{\sigma_e}{g}\,\epsilon_p\left(\frac{3\mathbf{S}}{2q}+\frac{\eta\mathbf{I}}{3}\right). \tag{2}$$

Relation (2) is the small strain rigid-plastic version of the non-associated Drucker–Prager deformation theory derived by Durban and Fleck (1997), subsequently employed along with the elastic branch in Durban and Papanastasiou (1997). Here $\boldsymbol{\epsilon}$ is the small strain tensor, σ_e and g are the effective stress and plastic potential defined by

$$\sigma_e=q+\mu\sigma_h,\quad g=q+\eta\sigma_h, \tag{3}$$

where q is the Mises effective stress and σ_h is the hydrostatic stress given by

$$q=\left(\tfrac{3}{2}\mathbf{S}\cdot\cdot\,\mathbf{S}\right)^{1/2},\quad \sigma_h=\tfrac{1}{3}\mathbf{I}\cdot\cdot\,\boldsymbol{\sigma}, \tag{4}$$

with $\mathbf{S}=\boldsymbol{\sigma}-\sigma_h\mathbf{I}$ denoting the stress deviator, $\boldsymbol{\sigma}$ is the usual stress tensor and $\mathbf{I}$ is the second-order unit tensor. The two parameters (μ,η) reflect the level of pressure sensitivity with the identity $\mu=\eta$ holding for associated materials and $\mu=\eta=0$ for the standard Mises solid. In other words, the Drucker–Prager

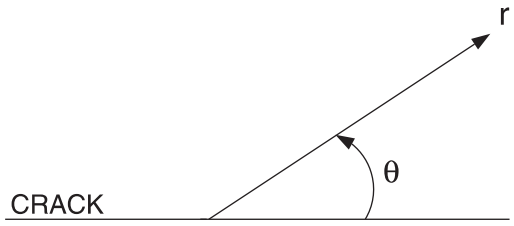

Fig. 1. Notation for plane strain mode-I crack tip field.

criterion (3), formulated in 1952, is a simple modification of the von Mises criterion, where the influence of a hydrostatic stress component, σ_h, on yield and failure is introduced by inclusion of an additional term in the von Misses expression, $\sigma_e = g = q$. The total plastic strain ϵ_p is a known function of the effective stress σ_e with the specific power law response,

$$\epsilon_p = \left(\frac{\sigma_e}{\sigma_0}\right)^n, \tag{5}$$

employed in this study. The hardening exponent n and reference stress σ_0 are experimentally determined material parameters. Mode I crack singular fields for the associated Drucker–Prager solid ($\mu = \eta$) have been studied by Li and Pan (1990).

Unlike the associated model, the more general version (2) does not admit a strain energy function. This is apparent from the specific plastic power relation, along the deformation path, for an elemental material volume,

$$\dot{W} = \boldsymbol{\sigma} \cdot\cdot \dot{\boldsymbol{\epsilon}} \tag{6}$$

where the superposed dot denotes rate of change with respect to, a time-like parameter. Thus, from Eq. (2)

$$\dot{W} = \sigma_e \dot{\epsilon}_p + \sigma_e \epsilon_p \dot{\ln}\left(\frac{\sigma_e}{g}\right) \tag{7}$$

with the second term clearly being non-holonomic when $\mu \neq \eta$ since then $\sigma_e \neq g$. For associated solids, with $g = \sigma_e$, we recover from Eq. (7), the strain energy function, $W = \int \sigma_e \, d\epsilon_p$, which is independent of the straining history. Put differently, with tensor $\boldsymbol{\gamma}$ denoting the deviatoric part of $\boldsymbol{\epsilon}$ in Eq. (2), in terms of the effective plastic shear strain,

$$\Gamma = \left(\frac{2}{3}\boldsymbol{\gamma} \cdot\cdot \boldsymbol{\gamma}\right)^{1/2} = \frac{\sigma_e}{g}\ \epsilon_p, \tag{8}$$

the plastic power (6) reads simply

$$\dot{W} = g\dot{\Gamma}. \tag{9}$$

However, in general, the plastic potential g cannot be expressed as a function of Γ alone, when the material is non-associated. In fact, while the complete elastoplastic strain invariants relations,

$$\Theta = \frac{\sigma_h}{\kappa} + \eta \frac{\sigma_e}{g}\epsilon_p, \tag{10}$$

$$\Gamma = \frac{q}{3G} + \frac{\sigma_e}{g}\epsilon_p, \tag{11}$$

where $\Theta = \operatorname{tr}\boldsymbol{\epsilon}$ is the volumetric strain, κ, the elastic bulk modulus and G, the elastic shear modulus, can in principle, be inverted to express (q, σ_h) in terms of (Γ, Θ), this will not be the case when the elastic branch is neglected. Indeed, with $(\kappa, G) \to \infty$, we find from Eqs. (10) and (11) the kinematic constraint,

$$\Theta = \eta\Gamma, \tag{12}$$

along with the duality, $g\Gamma = \sigma_e \epsilon_p$, which cannot be inverted to give (g, σ_e) in terms of Γ.

In the absence of a strain energy function associated with Eq. (2), there is no possibility of employing the path independent J integral (Rice, 1968), in conjunction with the power law (5), to deduce a-priori the stress singularity level at the near tip field, as has been done for the associated case by Li and Pan (1990). However, the algebraic structure of the constitutive relation (2) suggests a separation of variables singular field, along the same lines as the HRR solution (Hutchinson, 1968a,b; Rice and Rosengren, 1968), viz.

$$\sigma_r = r^s\tilde{\sigma}_r, \quad \sigma_\theta = r^s\tilde{\sigma}_\theta, \quad \sigma_{r\theta} = r^s\tilde{\sigma}_{r\theta}, \quad \sigma_z = r^s\tilde{\sigma}_z, \tag{13}$$

where $(\sigma_r, \sigma_\theta, \sigma_{r\theta}, \sigma_z)$ are the polar stress components, the tilde marks circumferential stress profiles and s, which is expected to be negative, is the stress singularity level. Likewise, we shall use the relations,

$$q = r^s\tilde{q}, \quad \sigma_{\mathrm{h}} = r^s\tilde{\sigma}_{\mathrm{h}}, \quad \sigma_{\mathrm{e}} = r^s\tilde{\sigma}_{\mathrm{e}}, \quad g = r^s\tilde{g}, \tag{14}$$

where, again, tilted quantities depend only on θ.

The plane strain constraint dictates that $\boldsymbol{\epsilon}$ in Eq. (2) has no active component in the z direction. Hence,

$$3(\tilde{\sigma}_z - \tilde{\sigma}_{\mathrm{h}}) + \tfrac{2}{3}\eta\tilde{q} = 0, \tag{15}$$

which, in turn, yields the Mises stress profile,

$$\tilde{q} = \left(\frac{3}{1-\eta^2/9}\right)^{1/2}\left[\left(\frac{\tilde{\sigma}_r - \tilde{\sigma}_\theta}{2}\right)^2 + \tilde{\sigma}_{r\theta}^2\right]^{1/2}, \tag{16}$$

and the hydrostatic stress profile,

$$\tilde{\sigma}_{\mathrm{h}} = \frac{1}{2}(\tilde{\sigma}_r + \tilde{\sigma}_\theta) - \frac{\eta}{9}\tilde{q}. \tag{17}$$

The axial stress, effective stress and plastic potential are as follows:

$$\tilde{\sigma}_z = \frac{1}{2}(\tilde{\sigma}_r + \tilde{\sigma}_\theta) - \frac{\eta}{3}\tilde{q}, \tag{18}$$

$$\tilde{\sigma}_{\mathrm{e}} = \left(1 - \frac{\mu\eta}{9}\right)\tilde{q} + \frac{\mu}{2}(\tilde{\sigma}_r + \tilde{\sigma}_\theta), \quad \tilde{g} = \left(1 - \frac{\eta^2}{9}\right)\tilde{q} + \frac{\eta}{2}(\tilde{\sigma}_r + \tilde{\sigma}_\theta). \tag{19}$$

The (r, θ) components of the displacements within the singular plastic zone, denoted by (u, v), are assumed to admit a separation of variables presentation analogous to Eq. (13), namely

$$u = kr^{ns+1}\tilde{u}, \quad v = kr^{ns+1}\tilde{v} \tag{20}$$

with

$$k = \sigma_0^{-n}. \tag{21}$$

Thus, the total plastic strain (5) is given by

$$\epsilon_{\mathrm{p}} = kr^{ns}\tilde{\sigma}_{\mathrm{e}}^n. \tag{22}$$

It is now a matter of ease to show that the tensorial equation (2) is reduced to three scalar equations that are independent of the radial coordinate, viz.

$$(ns+1)\tilde{u} = \frac{\tilde{\sigma}_{\mathrm{e}}^{n+1}}{\tilde{g}}\left[\frac{3}{2\tilde{q}}\left(\frac{\tilde{\sigma}_r - \tilde{\sigma}_\theta}{2}\right) + \frac{\eta}{2}\right], \tag{23}$$

$$\tilde{u} + \tilde{v}' = \frac{\tilde{\sigma}_{\mathrm{e}}^{n+1}}{\tilde{g}}\left[\frac{3}{2\tilde{q}}\left(\frac{\tilde{\sigma}_\theta - \tilde{\sigma}_r}{2}\right) + \frac{\eta}{2}\right], \tag{24}$$

$$\frac{1}{2}(\tilde{u}' + ns\tilde{v}) = \frac{\tilde{\sigma}_{\mathrm{e}}^{n+1}}{\tilde{g}}\left[\frac{3}{2\tilde{q}}\tilde{\sigma}_{r\theta}\right] \tag{25}$$

with the two following additional equations obtained from equilibrium requirements,

$$(s+1)\tilde{\sigma}_r + \tilde{\sigma}'_{r\theta} - \tilde{\sigma}_\theta = 0, \tag{26}$$

$$(s+2)\tilde{\sigma}_{r\theta} + \tilde{\sigma}'_\theta = 0, \tag{27}$$

where the prime denotes differentiation with respect to θ.

The system of five equations (23)–(27) with five unknown functions $(\tilde{u}, \tilde{v}, \tilde{\sigma}_r, \tilde{\sigma}_\theta, \tilde{\sigma}_{r\theta})$ is of the fourth order and is supplemented by two stress free boundary conditions along the crack face and by two mode-I symmetry conditions ahead of the crack; thus,

$$\begin{array}{lll} \theta = 0 & \tilde{v} = 0, & \tilde{\sigma}_{r\theta} = 0, \\ \theta = \pi & \tilde{\sigma}_\theta = 0, & \tilde{\sigma}_{r\theta} = 0. \end{array} \tag{28}$$

The eigensystems (23)–(28) admits non-trivial solutions only for discreet real values of the singularity s which serves as the eigenvalue of each eigenfield. Once an appropriate eigenvalue has been determined, the entire near tip field can be mapped up to one unknown constant. It follows that within the singular zone, the loading path is proportional, i.e. all stress components increase in a fixed ratio, implying that Eq. (7) is reduced to $\dot{W} = \sigma_e \dot{\epsilon}_p$, because σ_e/g remains constant along the loading history. It is therefore possible to calculate the strain energy, W, for both flow and deformation theories within the singular zone. This observation may suggest that the resulting stress singularity should not differ much from the HRR result of $s = -1/(n+1)$ (Li and Pan, 1990).

A lower bound on the eigenvalue s is provided through the requirement of vanishing plastic power within a small circle around the tip as its radius approaches zero. This condition imposes the bound, $s > -2/(n+1)$, on the singularity level. However, the requirement that the displacements, (20) should remain finite as $r \to 0$ along any direction suggests the lower bound is $-1/n$. Therefore, we seek, the strongest singularity within the bounds,

$$-\frac{1}{n} < s < 0. \tag{29}$$

3. Eigenfield calculation and illustration

The governing systems (23)–(28) has been solved numerically for $0 \le \theta \le \pi$ over a range of material parameters, (μ, η, n), to trace the eigenfield, which corresponds to the strongest permissible singularity. The search for eigensolutions was carried out by combining a Galerkin finite element scheme with a minimization subroutine for eliminating the oscillatory error in the eigenfield solution caused by deviation from the correct singularity. Indeed, testing the numerical procedure using the HRR singularity, we found that small deviations from the singularity value results in oscillations of the calculated eigenfield solution.

Table 1 shows the variation of eigenvalue, s, with the hardening exponent, n, and pressure sensitivity parameters, (μ, η). As expected, the HRR singularity, $s = -1/(n+1)$, is recovered for all associated cases, but otherwise the singularity level increases with the non-associativity measure, $(\mu - \eta)$. The trend is illustrated in Fig. 2 with $n = 10$ and in Fig. 3 where in Table 1 results have been lumped into a single parameter $(n+1)(\mu - \eta)s$. Deviations from the HRR values appear to be consistently appreciable with increasing levels of $(\mu - \eta)$.

The range of parameters, (μ, η), for which a separation of variables solution (13) exists, for the given n, is limited by the onset of a plastic potential corner zone ahead of the crack, when $\tilde{\sigma}_r = \tilde{\sigma}_\theta$, at $\theta = 0$. This observation, originally due to Li and Pan (1990), has been verified in our numerical calculations, though we have not traced the bounding (μ, η, n) surface, all results presented in this study are within the physically permissible space of solutions. A possible procedure for avoiding the stress path reaching the apex of the

Table 1
Singularity level for different material parameters

n	μ	η	$-s$
3	**0.1**	**0.1**	**0.25**
3	0.1	0.05	0.2547741
3	0.1	0.0	0.2596238
3	**0.15**	**0.15**	**0.25**
3	0.15	0.1	0.2545762
3	0.15	0.075	0.2568648
3	0.15	0.05	0.2591883
10	**0.1**	**0.1**	$\mathbf{9.09090 \times 10^{-2}}$
10	0.1	0.05	9.28390×10^{-2}
10	0.1	0.0	9.46833×10^{-2}
10	**0.2**	**0.2**	$\mathbf{9.09090 \times 10^{-2}}$
10	0.2	0.1	9.44541×10^{-2}
10	0.2	0.05	9.61487×10^{-2}
10	0.2	0.0	9.78496×10^{-2}
10	**0.4**	**0.4**	$\mathbf{9.09090 \times 10^{-2}}$
10	0.4	0.3	9.40825×10^{-2}
10	0.4	0.2	9.70777×10^{-2}
10	0.4	0.15	9.85829×10^{-2}
10	**0.6**	**0.6**	$\mathbf{9.09090 \times 10^{-2}}$
10	0.6	0.5	9.37663×10^{-2}
10	0.6	0.45	9.51185×10^{-2}
10	0.6	0.4	9.64452×10^{-2}
10	0.6	0.3	9.91008×10^{-2}
20	**0.3**	**0.3**	$\mathbf{4.76190 \times 10^{-2}}$
20	0.3	0.2	4.93495×10^{-2}
20	**0.5**	**0.5**	$\mathbf{4.76190 \times 10^{-2}}$
20	0.5	0.4	4.92043×10^{-2}
50	**0.8**	**0.8**	$\mathbf{1.96078 \times 10^{-2}}$
50	0.8	0.75	1.99181×10^{-2}

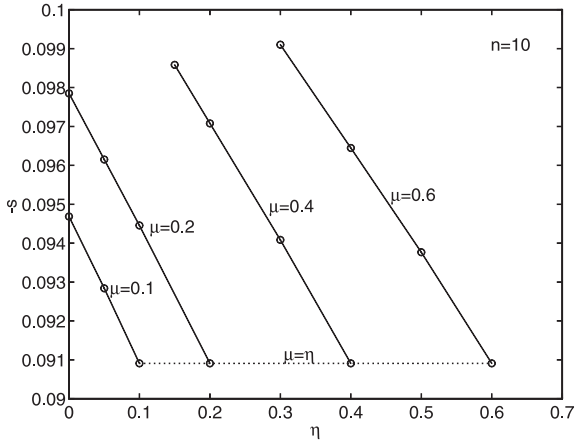

Fig. 2. Singularity level for non-associated solids with hardening exponent $n = 10$. Associated values are connected by broken line.

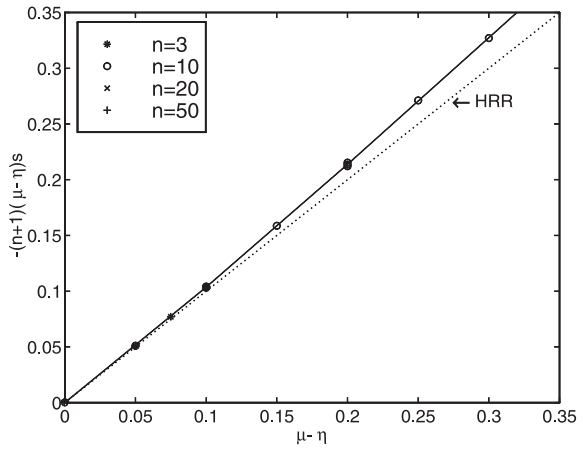

Fig. 3. Deviations of singularity level from HRR results with increasing non-associativity $(\mu - \eta)$.

Drucker–Prager plastic potential, suggested recently by Chang and Pan (1997), is to eliminate the apex altogether by rounding off the potential surface near the vertex.

Representative stress, strain and displacement profiles are displayed in Figs. 4–9. Stress components have been scaled so as to have $\tilde{\sigma}_r(\theta = 0) = 1$, whereas the strain profiles were evaluated from the standard definitions,

$$\tilde{\epsilon}_r = (ns + 1)\tilde{u}, \quad \tilde{\epsilon}_\theta = \tilde{u} + \tilde{v}', \quad \tilde{\epsilon}_{r\theta} = \tfrac{1}{2}(\tilde{u}' + ns\tilde{v}). \tag{30}$$

For associated materials, we find that the stress and strain profiles in Figs. 4–9 are in agreement with the earlier calculations in Li and Pan (1990). Non-associativity does not appear to have much influence on stress profiles (Figs. 4 and 7), but it does influence the strain (Figs. 5 and 8) and displacement (Figs. 6 and 9) distributions. Noticeable in particular is the shear strain $\tilde{\epsilon}_{r\theta}$, at large values of n (Fig. 8), when it becomes significantly higher for non-associated solids. Also at large n, the displacement may behave quite differently, when η is different from μ, as seen in Fig. 9.

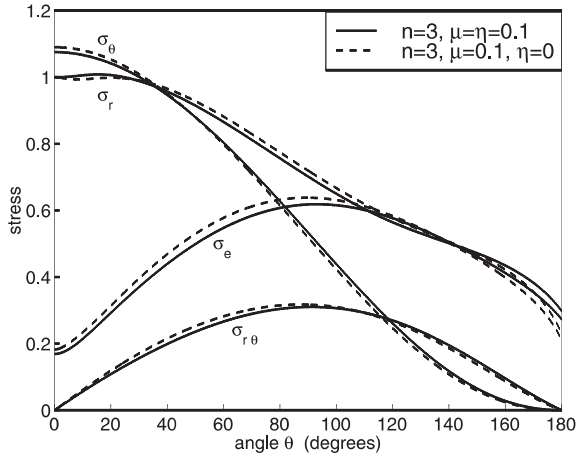

Fig. 4. Crack-tip stress eigenfields for associative $\mu = \eta = 0.1$ (—) and non-associative, $\mu = 0.1,\ \eta = 0$ (– – –) solids, $n = 3$.

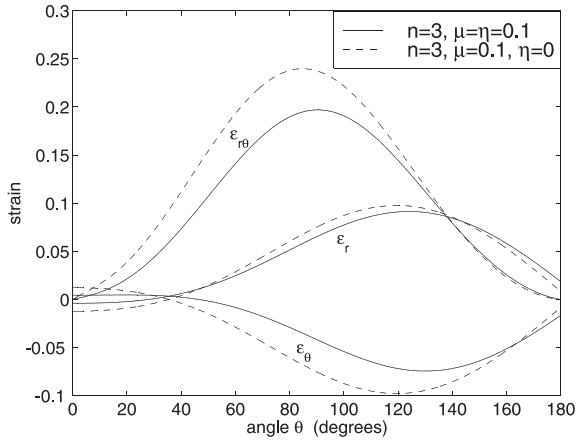

Fig. 5. Crack-tip strain eigenfields for associative $\mu = \eta = 0.1$ (—) and non-associative, $\mu = 0.1$, $\eta = 0$ (– – –) solids, $n = 3$.

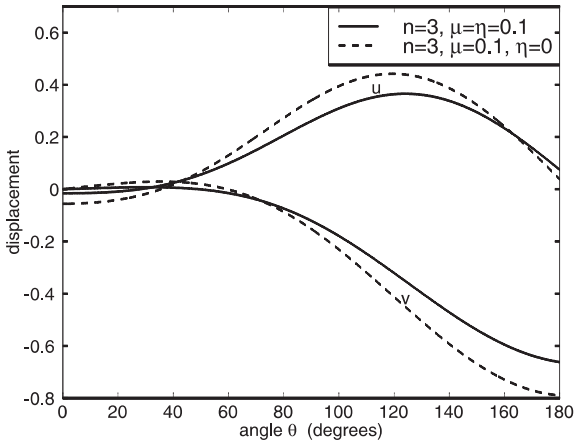

Fig. 6. Crack-tip displacement eigenfields for associative $\mu = \eta = 0.1$ (—) and non-associative, $\mu = 0.1$, $\eta = 0$ (– – –) solids, $n = 3$.

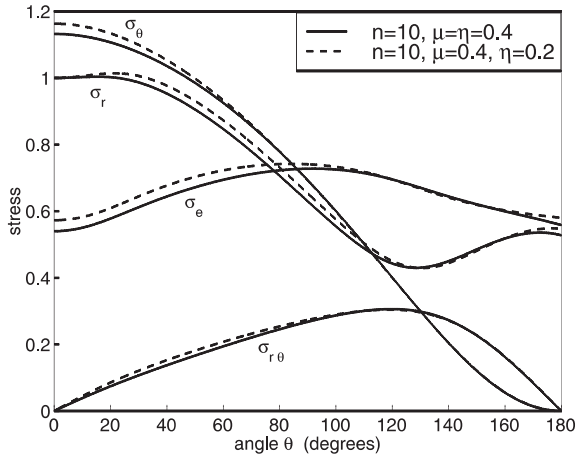

Fig. 7. Crack-tip stress eigenfields for associative $\mu = \eta = 0.4$ (—) and non-associative, $\mu = 0.4$, $\eta = 0.2$ (– – –) solids, $n = 10$.

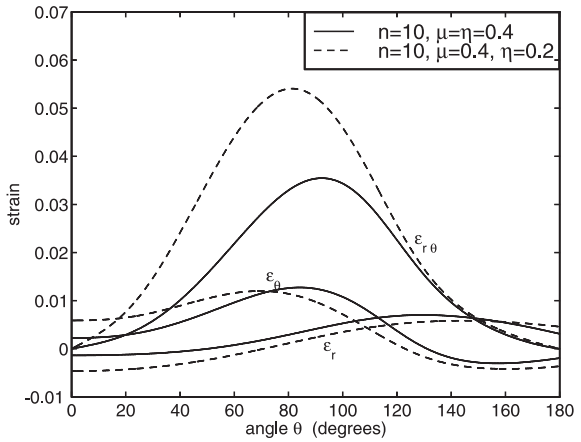

Fig. 8. Crack-tip strain eigenfields for associative $\mu = \eta = 0.4$ (—) and non-associative, $\mu = 0.4,\ \eta = 0.2$ (– – –) solids, $n = 10$.

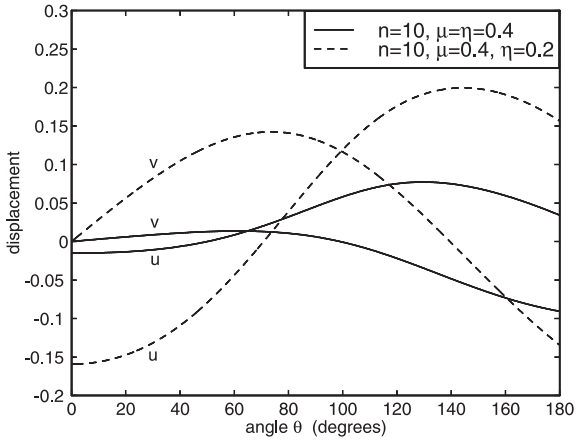

Fig. 9. Crack-tip displacement eigenfields for associative $\mu = \eta = 0.4$ (—) and non-associative, $\mu = 0.4,\ \eta = 0.2$ (– – –) solids, $n = 10$.

An interesting observation in the latter context follows from the data of Fig. 3 which can be approximated by the curve,

$$s = -\frac{1}{1+n}\left[1 + a(\mu-\eta) + b(\mu-\eta)^2 + \cdots\right], \tag{31}$$

with $a = 0.4094$ and $b = -0.3455$. It follows that the coefficient $(ns + 1)$ in Eq. (30) becomes very small and eventually changes its sign near the identity,

$$a(\mu-\eta) + b(\mu-\eta)^2 + \cdots = \frac{1}{n}, \tag{32}$$

implying via Eq. (20) that the displacements may become unbounded as $r \to 0$, if the non-associativity parameter, $(\mu - \eta)$, exceeds Eq. (32). However, numerical data beyond the limit (32) follow the trend given by the fitting expression (31) since mathematically all data reflect possible eigensolutions of the governing system.

Contours of constant effective stress, $\tilde{\sigma}_e$, as evaluated from Eq. (19) are shown in Figs. 10 and 11 for $n = 3$ and $n = 10$, respectively. As expected from the level of singularity, the contours of the effective stress suggest that the size of the plastic zone is larger for the non-associative case. The effective stress retains its basic plane strain shape, though the influence of non-associativity appears to increase, resulting in an extension of the plastic zone along the crack faces, for large n (Fig. 10). This is mainly due to the shift of the Mises stress, $\tilde{q}$, towards the crack for higher values of $(\mu - \eta)$. We found that the hydrostatic stress area is more sensitive to deviations from associativity for large n rather than small n, but in all cases it essentially dominates the zone ahead of the crack.

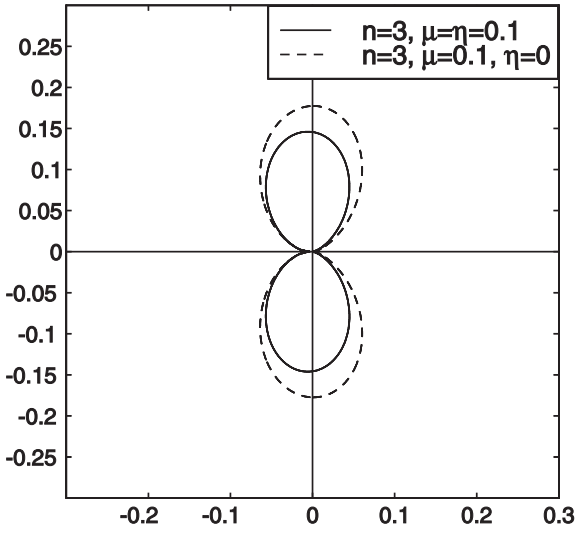

Fig. 10. Contours of effective stress, $\tilde{\sigma}_e$ for associative $\mu = \eta = 0.1$ (—) and non-associative, $\mu = 0.1$, $\eta = 0$ (– – –) solids, $n = 3$.

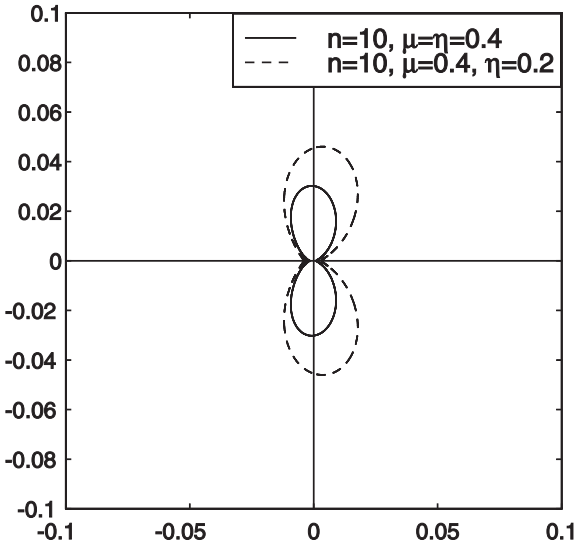

Fig. 11. Contours of effective stress, $\tilde{\sigma}_e$ for associative $\mu = \eta = 0.4$ (—) and non-associative, $\mu = 0.4$, $\eta = 0.2$ (– – –) solids, $n = 10$.

4. Concluding remarks

Eigenfields generated by systems (23)–(28) are restricted by bounds (29) that set a limit on the permissible level of non-associativity, via Eq. (32), which admits separation of variables eigenfields. Another limit is induced by the onset of plastic potential corner zone ahead of the crack where the constitutive relation (2) becomes invalid. A helpful observation in this context follows from the radial relation (23) when specified at $\theta = 0$. Since ahead of the crack $\tilde{\sigma}_{r\theta} = 0$ and from the numerics, $\tilde{\sigma}_\theta > \tilde{\sigma}_r$, we have from Eqs. (16) and (23) that at $\theta = 0$,

$$(ns+1)\tilde{u} = \frac{\tilde{\sigma}_{\mathrm{e}}^{n+1}}{\tilde{g}}\left[-\frac{3}{2}\left(\frac{1-\eta^2/9}{3}\right)^{1/2}+\frac{\eta}{2}\right]. \tag{33}$$

So, when the surface potential apex is hit with $\tilde{\sigma}_r = \tilde{\sigma}_\theta = \tilde{p}$, with $\tilde{p} > 0$ denoting the hydrostatic tension ahead of the crack, relation (33) reads

$$(ns+1)\tilde{u}(\theta=0) = \frac{\mu^{n+1}}{2\eta}\left[\eta-(3-\eta^2/3)^{1/2}\right]\tilde{p}^n. \tag{34}$$

This expression serves as the "corner" limit of validity on the physical plausibility of the eigensolutions.

It will be appreciated from Eq. (31) that HRR singularity levels provide a good estimate of the actual value of s for the non-associated Drucker–Prager solid. It remains an open question however whether a similar observation will emerge for other material models that do not admit a strain energy function. An interesting constitutive relation which may deserve further study is based on the elliptically shaped effective stress and plastic potential defined by

$$\sigma_{\mathrm{e}}^2 = q^2 + \alpha\sigma_{\mathrm{h}}^2, \quad g^2 = q^2 + \beta\sigma_{\mathrm{h}}^2 \tag{35}$$

with α and β denoting pressure sensitivity parameters. The usual construction of deformation theory based on Eq. (35) gives the constitutive law,

$$\boldsymbol{\epsilon} = \frac{3\sigma_{\mathrm{e}}\epsilon_{\mathrm{p}}}{2g^2}\left(\mathbf{S}+\frac{2\beta}{9}\sigma_{\mathrm{h}}\mathbf{I}\right), \tag{36}$$

which can be used for an eigenfield analysis when ϵ_{p} is a pure power of σ_{e}. The plastic power of Eq. (36) is again expressed by Eq. (7), but with σ_{e} and g given in Eq. (35), so no strain energy function exists for this material when $\alpha \neq \beta$. However, eigenfields are not restricted here by the onset of a corner zone, since the potential surfaces g in Eq. (35) are smooth, and a broader range of solutions may be mapped to assess the influence of non-associativity on singular near-tip fields in the absence of a strain energy function. In fact, the family (35) can be generalized by,

$$\sigma_{\mathrm{e}}^m = q^m + \alpha\sigma_{\mathrm{h}}^m, \quad g^m = q^m + \beta\sigma_m^2, \qquad \text{for } m = 3,4,\ldots \tag{37}$$

to facilitate studies of singular fields in non-associated materials.

Acknowledgements

The authors wish to thank Schlumberger Cambridge Research for supporting this research. A part of this study was supported by the fund for promotion of research at the Technion.

References

Bigoni, D., Radi, E., 1993. Mode I crack propagation in elastic–plastic pressure-sensitive materials. Int. J. Solids Struct. 30 (7), 899–919.

Chang, W.J., Pan, J., 1997. Effects of yield surface shape and round-off vertex on crack-tip fields for pressure-sensitive materials. Int. J. Solids Struct. 34, 3291–3320.

Durban, D., Fleck, N.A., 1997. Spherical cavity expansion in a drucker–prager solid. J. Appl. Mech. 64, 743–750.

Durban, D., Papanastasiou, P., 1997. Elastoplastic response of pressure sensitive solids. Int. J. Num. Anal. Meth. Geomech. 21, 423–441.

Hutchinson, J.W., 1968a. Singular behaviour at the end of a tensile crack in a hardening material. J. Mech. Phys. Solids 16, 13–31.

Hutchinson, J.W., 1968b. Plastic stress and strain fields at a crack tip. J. Mech. Phys. Solids 16, 337–347.

Li, F.Z., Pan, J., 1990. Plane-strain crack-tip fields for pressure-sensitive dilatant materials. J. Appl. Mech. 57, 40–49.

Papanastasiou, P., 1997. The influence of plasticity in hydraulic fracturing. Int. J. Fract. 84, 61–97.

Papanastasiou, P., 1999. The effective fracture toughness in hydraulic fracturing. Int. J. Fract. 96, 127–147.

Rice, J.R., 1968. A path independent integral and the approximate analysis of strain concentration by notches and cracks. J. Appl. Mech. 35, 379–386.

Rice, J.R., Rosengren, G.F., 1968. Plane strain deformation near a crack tip in a power law hardening material. J. Mech. Phys. Solids 16, 1–12.

Yuan, H., Lin, G., 1993. Elastoplastic crack analysis for pressure-sensitive dilatant materials. Part I: Higher-order solutions and two-parameter characterization. Int. J. Fract. 61, 295–330.